International Journal of Scientific Engineering and Applied Science (IJSEAS) – Volume-3, Issue-12, Dec 2017
ISSN: 2395-3470
www.ijseas.com

Thermal Influence on Airfoil Hydrodynamic Boundary Layer: Part 1-Theoretical Analysis

Miguel Toledo-Velázquez, Alfredo Pérez-Montiel, Juan Abugaber-Francis, Guilibaldo Tolentino-Eslava
Instituto Politécnico Nacional, Escuela Superior de Ingeniería Mecánica y Eléctrica. Sección de Estudios de Posgrado e Investigación. Laboratorio de Ingeniería Térmica e Hidráulica Aplicada (LABINTHAP). Unidad Profesional "Adolfo López Mateos", Edif. 5, 3er piso, Col. Lindavista, C.P 07738, Ciudad de México, México.

ABSTRACT
The present paper presents a theoretical analysis that corresponds to a first part of a complete investigation about the thermal influence on airfoil hydrodynamic boundary layer. Compressor rotating stall is analyzed, specifically the principles of aerodynamics and airfoil stall, and rotating stall in compressor blading. Also, foundations on hydrodynamic boundary layer that include laminar and turbulent boundary layer, boundary layers in airfoils and boundary separation are addressed. There is a theoretical analysis about thermal boundary layer and heat transfer. The basis presented is of great importance for the correct understanding and implementation of the last addressed topic that deals with a test case study where many numerical simulations are carried out.
Keywords: *Thermal Influence, Airfoil, Hydrodynamic Boundary Layer, Numerical Simulation*

1. INTRODUCTION

In turbomachinery applications, axial flow compressors are used to provide a gas flow with high pressure ratios. A compressor consists of several stages each of them formed by a rotor and a stator stage. Often at the input of the axial compressor a blade arrangement is placed called directive to ensure that air enters the angle designed to the first rotor stage. Its operation mainly consists of accelerating the fluid through a cascade of blades rotors blades and later scattered in a cascade of stators vanes to obtain a pressure increase. The diffusion in the stator converts the velocity increase obtained in the rotor cascade into pressure increase. The flow within the axial compressor is always subject to an adverse pressure gradient, which marks an important point of study, since the possibility of stall on the surface in a blade is latent leading to a phenomenon known as stall. The airfoils used in the compressor disks are designed considering this problem; however, it is important to investigate alternative solutions to avoid such effect.

One aspect that favors the stall is certainly the flow instability within the boundary layer that causes its separation from the airfoil surface. Since the adverse pressure gradient existing in the process, there is a flow deceleration due to the change of direction of the airfoil surface, making the presence of flow separation even more imminent. Two of the physical properties of fluids strongly related to the boundary layer, are undoubtedly the dynamic viscosity and density. The dynamic viscosity is the constant that is directly related to the shear strengths within the fluid. This property, in turn, is directly affected by the variation of fluid temperature. Therefore, it can be deduced that a temperature reduction in the viscous zone of the fluid, results in a reduction in the dynamic viscosity. This produces a reduction of shear strengths giving the fluid greater stability and delaying or avoiding the presence of stall.

The investigation proposed deals with the thermal influence on airfoil hydrodynamic boundary layer and is divided into two studies. The first one, which is presented in this paper, is the literature review needed for the complete analysis and addresses: compressor rotating stall principles, and a theoretical analysis about hydrodynamic and thermal boundary layers. The second one is a test case study.

2. COMPRESSOR ROTATING STALL

2.1 Principles of aerodynamics and airfoil stall

When an isolated airfoil is parallel to the air flow velocity, current lines are developed by dividing around the body, starting from the leading edge, and reattach at the exit edge of the body, as shown in Figure 1. The mainstream does not suffer any deflection due to the presence of the airfoil. Through

the local distribution of the stream and the fluid friction on the surface, forces are exerted on the airfoil. If the airfoil has been well designed, the flow will be orderly or non-turbulent.

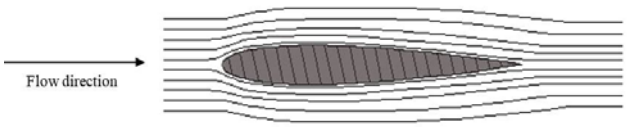

Figure 1. Air flow around an airfoil with angle of inclination equal to zero [1].

If the airfoil is placed at an angle of attack relative to the flow stream, a flow disturbance created by its presence is generated and the stream line pattern will change. The air is subjected to a local deflection, at a posterior distance to the back surface of the body, where the flow is still parallel and uniform. Local deflection of the flow stream can be calculated by Newton's laws only if the airfoil exerts a force on the air. The reaction of the air will produce an equal and opposite force on the airfoil. These forces may appear only in the form of a stream pressure on the airfoil. The presence of the blade changes the local pressure distribution with respect to the flow conditions that are anterior to the body. By examining the stream lines around the airfoil, as shown in Figure 2, the lines approach each other, indicating an increase in speed and a reduction in static pressure.

The pressure measurement at various points on the airfoil surface shows a pressure distribution as shown in Figure 3. The vectorial sum of these pressures produces resultant forces acting on the airfoil. These resultant forces can be decomposed into a lift component *L* at right angles with respect to undisturbed stream flow, and a drag component *D*, by moving the airfoil in the direction of fluid movement. It is assumed that these resultant forces act at a defined point located in the blade, so the behavior is the same as if all the individual components acted simultaneously.

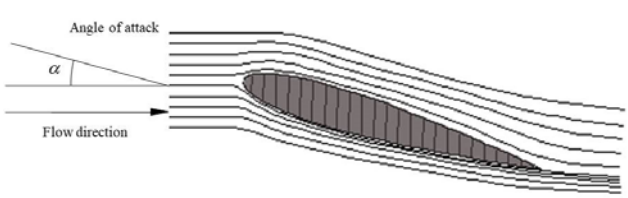

Figure 2. Air flow around an airfoil with angle of inclination α [1].

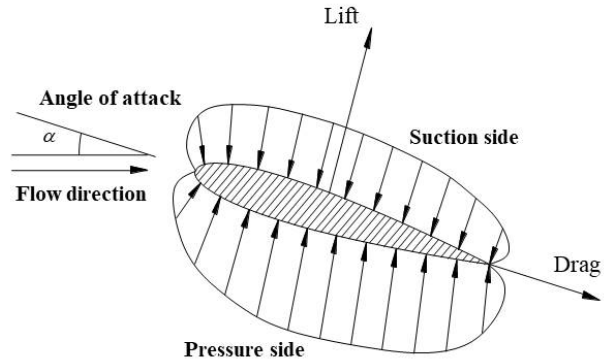

Figure 3. Pressure distribution and forces acting on airfoil surface [1].

The value of the lift (L) and drag (D) forces can be measured experimentally for all values of flow velocity, angle of attack and various airfoil shapes. For a specific airfoil, these forces can be represented as shown in Figure 4. It is also possible to define expressions for these forces as follows:

$$D = C_D A \rho \frac{U^2}{2} \tag{1}$$

$$L = C_L A \rho \frac{U^2}{2} \tag{2}$$

where C_L and C_D are the lift and drag coefficients, A is the area of the surface, ρ is the density of the fluid and U its velocity. The coefficients C_L and C_D can be calculated by experiments in a wind tunnel, and plotted as shown in Figure 5 with respect to the angle of attack. Examining Figure 5, it can be seen that there is an angle of attack in which the force and lift coefficient are maximal. If this angle is exceeded, stall is generated and the drag force increases rapidly. Since this maximum angle is approximated, a large percentage of the available energy is lost in overcoming the friction, provoking a reduction in efficiency. Therefore there is a point, usually prior to the point of maximum lift coefficient, in which the most economical operation occurs. Some factors that affect stall dynamics are the Reynolds number, the Mach number and the geometric shape of the body, although there are

others that affect to a lesser extent such as vortex effects and airfoil flexibility [2].

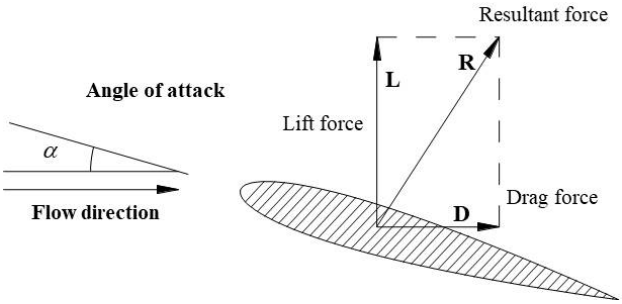

Figure 4. Representation of the forces acting on an airfoil [1].

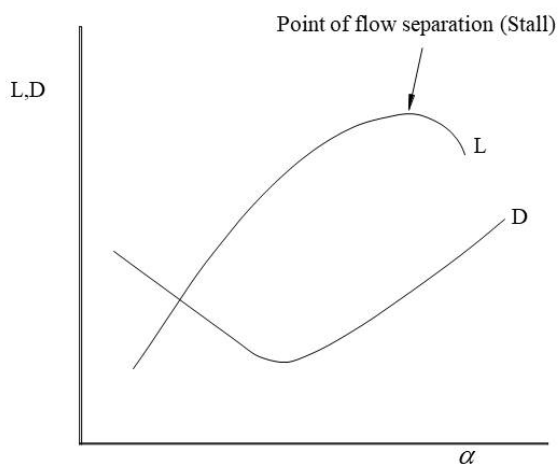

Figure 5. Behavior of lift and drag forces as a function of angle of attack.

2.2 Rotating stall in compressor blading

Rotating stall in compresor blading is an instability due to disturbance of the circular flow pattern, which begins with the flow separation on the surface of one or more airfoils and propagates around the compressor cincumference in a percentage of 20 to 70% of the rotor speed according to Greitzer (1980) [3], or 30 to 60% according to Hawthorne (1964) [2]. This phenomenon causes a reduction in the compressor pressure increase, and within the operating map of a compressor, corresponds to the area characterized as a blocking area. The blocking mechanism in compressor blading was exposed by Emmons et al. in 1955 [4], which is explained as follows. A cascade of compressor blades is considered with a high angle of attack as illustrated in Figure 6. Within the inlet flow there is an alteration in the flow uniformity which, together with the angle of attack of the airfoil, produces the optimum conditions for a stall condition on the suction surface of the blade *B*. The now separated fluid produces a blockage between airfoils *B* and *C*, causing a bifurcation of the inlet flow out of *B* towards *A* and *C*, resulting in an increase of the angle of attack of the blade *C* initiating a stall effect on its suction surface and generating a propagation of the blocking flow along the blading.

The phenomenon of propagation of the blockage in axial compressors was published openly in the years 1953 and 1954, proposing several theories to explain it; however, the equations of movement were linearized, limiting the analysis strictly to small perturbations, and the not-lineal characteristics were introduced in various forms, for an instant, for an interval or for abrupt changes in the lift coefficient.

It is possible to distinguish at least two types of blocking in cascades, full-span and part-span. The first one occurs when the separation obstructs the path of the fluid through the passage area of the blades, and the second one prevents flow only in a fraction of the annular area of passage of the blades. Probably, an effect with more importance than the reduction in the performance of the compressor, is the generation of loads in the blades. Rotating stall produces periodic forces on the rotor blades and stator vanes that are at least as large in magnitude as the dynamic loading of the fluid velocity at the designed angles of attack, generating noise and alterations in the operation of auxiliary equipment. The great magnitude of periodic forces combined with the number of possible blocked cells makes it difficult to avoid resonance and fatigue. In the case where the compressor reaches the maximum speed of rotation, it is very important to avoid the airfoil resonance because the greatest aerodynamic forces take place. The operation of axial compressors designed for high pressure ratios are most likely to suffer blockage in the early stages during the periods of initial operation. The blockage developed in the early stages of the compressor often advances axially towards the later stages and further reduces the expected performance of the compressor.

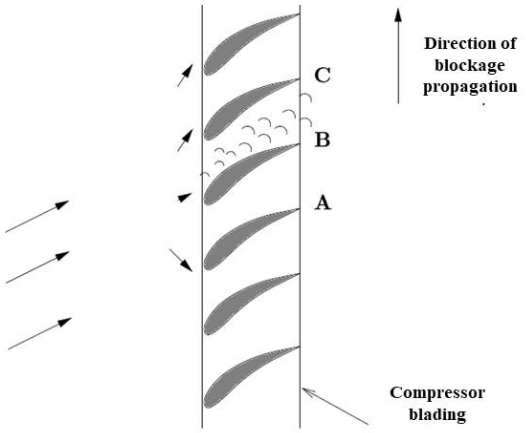

Figure 6. Physical mechanism of the start of rotating stall in compressor blading [4].

3. HYDRODINAMIC BOUNDARY LAYER

3.1 Laminar and turbulent boundary layers

Within the boundary layer two different flow types can be present: laminar and turbulent. Figure 7 shows the differences between the laminar and turbulent flow conditions. In the laminar boundary layer, the movement of the fluid is ordered and is possible to identify stream lines on which the particles travel. The movement of the fluid along the stream lines is characterized by velocity components in the x and y direction. Since the velocity component v is in the normal direction to the surface, it can contribute significantly to the transfer of momentum or energy through the boundary layer. Movement of normal fluid to the surface is necessary for the growth of the boundary layer in the direction x. In contrast, the fluid movement in the turbulent boundary layer is highly irregular and is characterized by velocity fluctuations. These fluctuations increase the transfer of momentum and energy, thus increasing surface friction and heat transfer ratio. Due to the fluid mixture resulting from the fluctuation, the thicknesses of the boundary layer are larger and the boundary layer profiles are thinner than in a laminar flow. The boundary layer is initially laminar, but at a distance from the leading edge small perturbations are amplified that cause the start of the transition to turbulent flow. Flow fluctuations become the transition region (in the three-dimensional case), and the boundary layer eventually becomes completely turbulent. In the fully turbulent region, conditions are characterized by high instability, three-dimensional movements of relatively large elements of fluid, and it is not surprising that the transition to turbulent flow is accompanied by significant increases in boundary layer thickness, the wall and the convection coefficient. These effects are illustrated in Figure 8 for the hydrodynamic boundary layer thickness δ and the local convection coefficient h. As can be seen, in the transition zone, there is a high uncertainty regarding the exact behavior of the system properties (fluid-body), such as h, which leads to a high uncertainty with respect to the values of the expressions that determine the thermal and hydrodynamic boundary layer thicknesses.

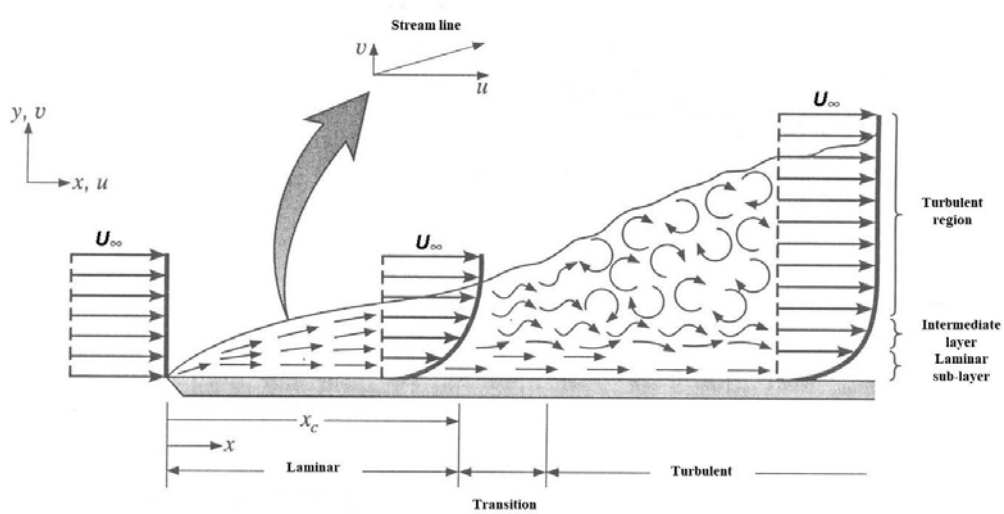

Figure 7. Development of the hydrodynamic boundary layer on a flat plate specifying flow rate zones [5].

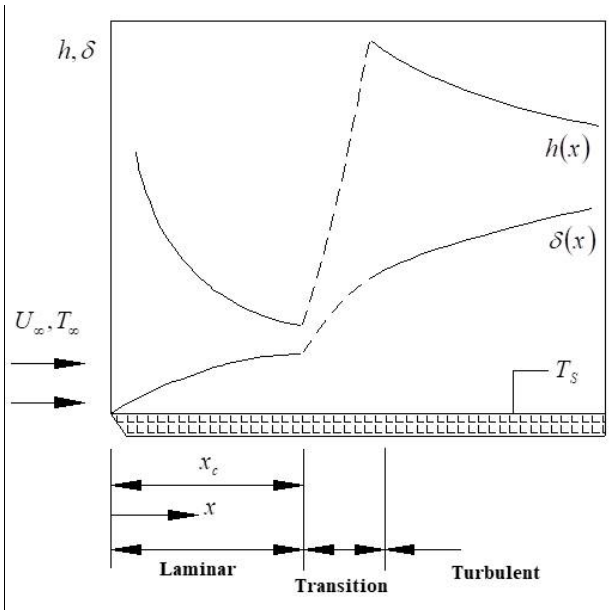

Figure 8. Thickness variation of the boundary layer δ and the local coefficient h of heat transfer for flows on an isothermal flat plate [5].

Laminar boundary layer

Flows with very small viscosities or very high Reynolds numbers will now be treated. For simplicity, le tus consider the flat flow of one of these fluids passing through a thin cylindrical body, as illustrated in Figure 9. The velocities are of the order of magnitude of the free-flow velocity U_∞ from the immediate zone to the surface of the body. Both the shape of the stream lines and the velocity distribution are almost identical to those of the non-viscous flow (potential flow). There is a transition from velocity equal to zero in the wall up to the nominal velocity which occurs at a certain distance from the wall.

The thickness δ of the boundary layer can be estimated as follows. As a consequence of the viscosity in the wall, the transport of momentum on this layer takes place with the velocity $U_v(\upsilon,\delta)$, which, for dimensional considerations is $U_v = \upsilon/\delta$. If t_B is a typical time in which the particle travels in the layer, we have the expression $\delta = U_v t_B$. Unifying the two previous expressions we have:

$$\delta \approx \sqrt{\upsilon \cdot t_B} \tag{3}$$

We conclude that the thickness of the boundary layer is proportional to the square root of the kinematic viscosity [1]. In the simplification of the the Navier-Stokes equations, it is assumed that this thickness will be very small compared to the characteristic length of the body l:

$$\delta \prec\prec l \tag{4}$$

Thus, the solution of the boundary layer equations has an asymptotic characteristic for very high Reynolds numbers. If the free-flow velocity U_∞ and a characteristic dimension l of the body are used as the reference, the relation $\delta \approx \sqrt{\upsilon}$ leads to the correct representation of:

$$\frac{\delta}{l} \approx \frac{1}{\sqrt{\mathrm{Re}}} \text{ with } \mathrm{Re} = \frac{Ul}{\upsilon} \tag{5}$$

Therefore, the boundary layer thickness tends to zero with increasing Reynolds number, taking as a limiting case $\mathrm{Re} \to \infty$, where the boundary layer actually disappears.

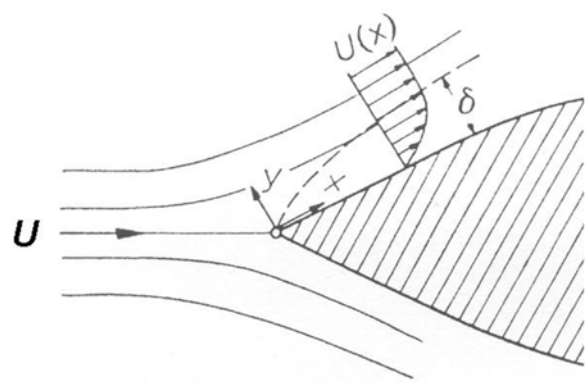

Figure 9. Boundary layer flow through a wall [5].

3.2 Boundary layer in airfoils

The boundary layer in a flat plate with any degree of inclination is particularly simple, from the external flow considered to be non-viscous and therefore, the limited solution is for translating flows with constant pressure throughout the field. However, in the case where the flow passes through a body with arbitrary geometry, additional pressure forces occur. Figure 10 shows the boundary layer on an airfoil, where, for reasons of clarity, the dimensions in the transverse direction are amplified. As with the plate, a laminar

boundary layer starts to develop at the beginning of the airfoil. After some distance x_{crit} along the contour of the body, the transition from laminar to turbulent occurs, so the boundary layer is turbulent for $x \succ x_{crit}$. Due to the geometry of the body, the non-viscous external flow leads to a pressure distribution at the outer edge of the boundary layer. This pressure distribution is "imposed" on the boundary layer at each point of x, the pressure perpendicular to the wall in the boundary layer is constant. Therefore the pressure distribution at the outer edge of the boundary layer is identical to the pressure distribution in the wall. A difference between these two pressure distributions can only occur from the curvature of the stream line and the resulting pressure gradient perpendicular to the main flow direction as a compensation for the centrifugal forces. Since the boundary layers are very thin compared to the radius of curvature of the body contour at high Reynolds numbers, the pressure gradient perpendicular to the wall does not occur. The pressure is imposed on the boundary layer by the external flow, and is only a function of x. In addition, the dependencies mentioned in the case of boundary layer in a plane are only valid: as the boundary layer develops along the contour of the body, in general, the thickness of the boundary layer $\delta(x)$ increases and the shear forces τ_w on the wall decrease. The increase in the thickness of the downstream boundary layer is greater in the case of turbulent boundary layer than laminar. As the Reynolds number formed by the free-flow velocity U_∞ and a characteristic length of the body l that increases, the thickness of the boundary layer decreases to zero in the limiting case Re $\rightarrow \infty$. The pressure distribution imposed by the external flow is of considerable importance in the formation of the boundary layer. For example, the transition from the laminar boundary layer to turbulent depends strongly on that. If the pressure gradient increases in the direction of flow, as may occur in the posterior region of the airfoil, or on the posterior coarse part of the body, it is possible that the boundary layer may be separated from the wall.

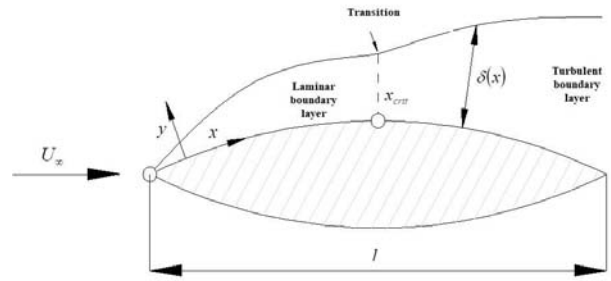

Figure 10. Development of the boundary layer on an airfoil, viscous external flow [5].

3.3 Boundary layer separation

When a fluid passes over a convex body, the thickness of the boundary layer will be zero upstream of the stagnation point and will grow as it moves downstream of that point. If the static pressure of the fluid around the surface area is constant or decreasing downstream, as in B and C of Figure 11, the layer will remain in contact with the surface over its entire length. If the flow conditions the velocity decreases along the surface, there is a development of an adverse pressure gradient rising the pressure near the surface in the downstream direction; then the shape of the velocity distribution near the surface passes from convex to concave as in D because the kinetic energy of the boundary layer decreases by the action of the adverse pressure gradient. When the velocity variation profile is tangent to the surface normal, as in D, the separation of the boundary layer begins. The point of separation is further away, downstream, when the movement is turbulent, than in the case of being laminar because the energy that has the turbulent boundary layer is greater; therefore, the turbulence of a stream is not always an inconvenience.

Beyond the point of separation, positive pressure (which increases downstream) results in upstream flow in the vicinity of the surface, and in the discontinuity surface between this upwardly moving layer and the mainstream which there is a small portion of rotating fluid. The adjacent portions will have to describe vortices which force the stream to move away from the wall, this can be seen in Figure 12. Eventually the largest vortices are released and moved downstream, being replaced by others in rapid succession.

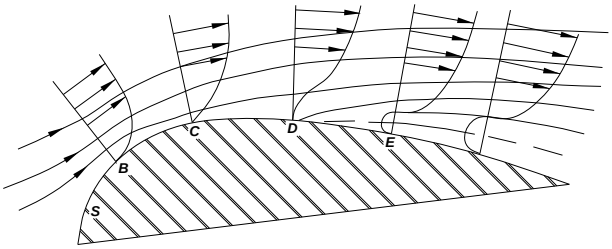

Figure 11. Boundary layer separation due to the adverse pressure gradient

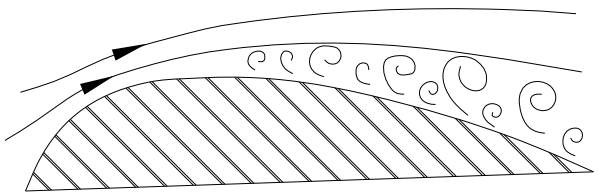

Figure 12. Formation of vórtices due to the boundary layer separation.

An important example of separation occurs in the flow surrounding an element with wing-shaped section. Along the upper surface of Figure 13, the pressure relative to that which exists at a great upstream distance varies from a large negative value (the stream lines are very close to one another and the pressure is small), to a positive value at the trailing edge. Consequently the absolute pressure along the upper face increases during this flow, or in other terms, there is an adverse pressure gradient. The separation does not occur for small angles of attack, but as the angle of incidence increases, this phenomenon ends up appearing. Eventually the lift begins to decrease with great increase of the resistance as that point moves forward.

Another type of boundary layer separation occurs at the posterior edge of a blade, where the boundary layer leaving the surface is transformed into a flow wake. The fluid slowly moves and constitutes the continuous wake retarding behind the body after passing the exit edge, but as the surface resistance has disappeared, the viscosity of the fluid now acts in the sense of rapidly unifying the profile of the velocity distribution, see Figure 14, by the energy exchange that accompanies the turbulence. However, it is evident that the wake of the fixed blades creates a flow field of regularly variable intensity at the entrance to the blading of a short distance downstream, and that the blades also produce a similar field with the exception that rotates around the axis of the compressor, to the entrance of the new stator vanes. These periodic fluctuations are the cause of vibrations.

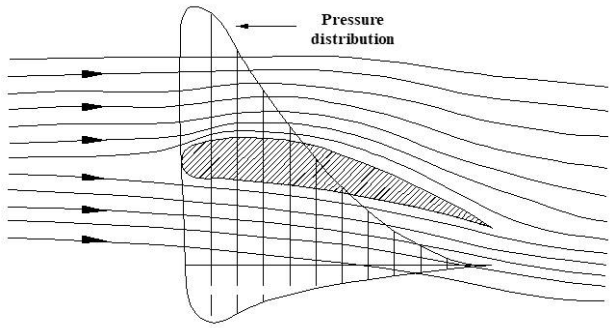

Figure 13. Pressure distribution of an airfoil immersed in a flow.

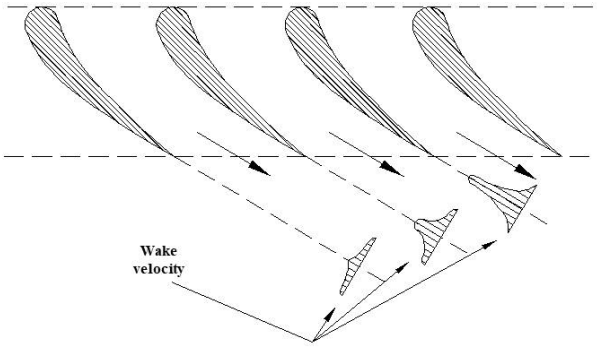

Figure 14. Velocity of flow wake behind the blades.

Since the equalization of the velocities in the wake means a small delay of the mainstream and a considerable acceleration of the material of the wake, a small flow takes place from the mainstream towards the region of the wake during the period of equalization. Conversely, the initial setting of the boundary layer and the subsequent delay of the fluid at the inlet edges of the surface produce a small flow at some distance from them. These phenomena form the basis for the definition of the aerodynamic body in which the boundary layer does not separate from its surface, or in which this phenomenon occurs so close to the trailing edge that the portions of separated fluid are so close behind the object that they form only a reduced wake. In a body whose shape is not aerodynamic, the resistance due to the separation is generally much greater than the caused by the friction in the walls. The roughness of the surfaces increases the losses due to the effects described above, worsening the separation of the flow, decreasing the transition speed and increasing

the energy of the flow vortices. The presence of non-uniform turbulence in the post-curvature fluid generally adversely affects flow through the blades of the contiguous blading, resulting in losses in the subsequent elements. The separation of the boundary layer occurs easily if there is an increase in the pressure gradient in the direction of flow; it can occur if the pressure is constant, but it is less likely to occur if the pressure decreases, as in the case of a divergent nozzle. Hence in a cascade of blades within an axial compressor, this phenomenon will frequently appear.

4. THERMAL BOUNDARY LAYER AND HEAT TRANSFER

4.1 Thermal boundary layer in laminar regime

In the same manner that a hydrodynamic boundary layer develops when there is a flow of a fluid on a surface; a thermal boundary layer must be developed if there is a temperature gradient between the free flow and the surface. Consider a flow on an isothermal flat plate. At the entry edge, the speed profile is uniform (Figure 15), $T(y) = T_\infty$. However, the particles coming into contact with the plate, reach thermal equilibrium at the surface temperature of the plate. In turn, these particles exchange energy with the adjacent layers, developing temperature gradients in the fluid. The region of the fluid in which these temperature gradients exist is known as the thermal boundary layer and its thickness is typically defined as:

$$\left[\frac{T_S - T}{T_S - T_\infty}\right] = 0.99 \qquad (6)$$

With the increase in distance from the inlet edge, the heat transfer effects penetrate the free flow of the stream, increasing the thickness of the thermal boundary layer.

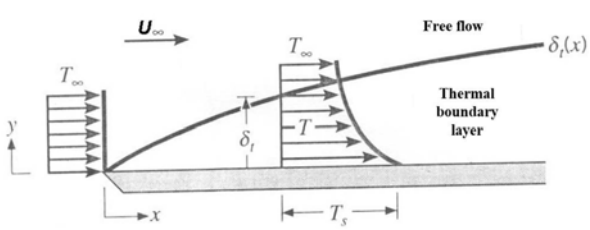

Figure 15. Development of a boundary layer on isothermal flat plate [5].

The relationship between this boundary layer and the convective heat transfer coefficient can be demonstrated. At any distance x from the leading edge, the heat flow can be obtained by the Fourier law between the plate and the fluid, with $y = 0$. This is:

$$q_S'' = -k_f \left.\frac{\partial T}{\partial y}\right|_{y=0} \qquad (7)$$

This expression is adequate because there is no fluid movement on the surface and the energy transfer occurs only by conduction. If we combine Equation 7 with Newton's law of cooling which states that:

$$q'' = h(T_S - T_\infty) \qquad (8)$$

where h is the local convection coefficient formulated as:

$$h = \frac{-k_f \left.\partial T/\partial y\right|_{y=0}}{T_S - T_\infty} \qquad (9)$$

Therefore the conditions in the thermal boundary layer, which strongly influences the temperature gradient $\left.\partial T/\partial y\right|_{y=0}$, determine the rate of heat transfer through the boundary layer. If $(T_S - T_\infty)$ is constant, independent of x, while δ_t increases with the increment of x, the temperature gradients in the boundary layer should decrease with increments of x. Similarly, the magnitude of $\left.\partial T/\partial y\right|_{y=0}$ decreases with increments of x, and this means that q_S'' and h decrease with the growth of x.

4.2 Thermal boundary layer and flow velocity

Equations 10 and 11 are based on the hypothesis that velocity and temperature variations occur in the thin region near the solid wall. This assumption in no way implies that u and T reach the values of the free stream within the distance δ.

$$u\frac{\partial u}{\partial x} + v\frac{\partial u}{\partial y} = -\frac{1}{\rho}\frac{dP_\infty}{dx} + \nu\frac{\partial^2 u}{\partial y^2} \qquad (10)$$

$$u\frac{\partial T}{\partial x} + v\frac{\partial T}{\partial y} = \alpha\frac{\partial^2 T}{\partial y^2} \qquad (11)$$

where δ is the thickness of the region in which the velocity varies from 0 in the wall to the speed U_∞ of the free stream. δ_T is the thickness of another thin region in which T varies from T_0 in the wall to T_∞ in the free stream. In scalar terms, the friction of the fluid can be written as:

$$\tau \approx \mu \frac{U_\infty}{\delta} \tag{12}$$

Thus, to estimate the effort caused by the friction presented on the wall, the extent δ of this imaginary thin region should be evaluated. Consider the simplest free flow possible, namely a free stream with pressure gradient p_∞. (This is a very good approximation for the flow around the plate in a heat transfer area, because the pressure drop in the direction of flow is not significant over the length l dictated by the end of the plate). With $dp_\infty/dx = 0$, in Equation 10, the momentum equation of the boundary layer implies:

Inertia – Friction

$$\frac{U_\infty^2}{l}, \frac{vU_\infty}{\delta} \approx \upsilon \frac{U_\infty}{\delta^2} \tag{13}$$

Referring once again to mass continuity, we conclude that the two inertial terms are of the same order of magnitude. Therefore, Equation 13 requires:

$$\delta \approx \left(\frac{vl}{U_\infty}\right)^{1/2} \tag{14}$$

In other words

$$\frac{\delta}{l} \approx \frac{1}{\sqrt{\mathrm{Re}_l}} \tag{15}$$

where Re_l is the Reynolds number based on the longitudinal dimension of the hydrodynamic boundary layer region. Equation 15 is an important result: it states that the proposed thickness on which the boundary layer theory $(\delta << l)$ is based must be much less than the length, and is valid for $\mathrm{Re}_l^{1/2} >> 1$.

The scale of shear forces on the wall is:

$$\tau \to \mu \frac{U_\infty}{l} \mathrm{Re}_l^{1/2} \to \rho U_\infty^2 \mathrm{Re}_l^{-1/2} \tag{16}$$

So the coefficient of surface friction $C_f = \tau/\left(\frac{1}{2}\rho U_\infty^2\right)$ depends on the Reynolds number:

$$C_f \to \mathrm{Re}^{-1/2} \tag{17}$$

The issue of heat transfer is focused through the thickness of the thermal boundary layer δ_T

$$h \to \frac{k(\Delta T/\delta_T)}{\Delta T} \to \frac{k}{\delta_T} \tag{18}$$

Where $\Delta T = (T_0 - T_\infty)$ is the temperature variation in the region $\delta_T \times l$. The energy equation of the boundary layer states that there is always a balance between the convection-conduction phenomena.

$$u\frac{\Delta T}{l}, v\frac{\Delta T}{\delta_T} \to \frac{\Delta T}{\delta_T^2} \tag{19}$$

The thickness δ_T needed to estimate $h \to k/\delta_T$ can be determined analytically in the following two limits:

1. The thickness of the thermal boundary layer $\delta_T >> \delta$. At this limit, the layer δ_T is very small relative to the thickness of the hydrodynamic boundary layer measured in the same x value. The velocity u in the external side of δ (and inside of δ_T) is U_∞. According to the relationship $U_\infty/l \to v/\delta$, the velocity v in the same region is $v \to U_\infty \delta/l$. This means that the second term on the left side of Equation 19 is dominated by $U_\infty \Delta T/l$. In conclusion, the convection - conduction balance expressed by Equation 19 is $U_\infty \Delta T/l \to \alpha \Delta T/\delta_T^2$, from which

$$\frac{\delta_T}{l} \rightarrow Pe_l^{-1/2} \rightarrow \Pr^{-1/2} \operatorname{Re}_l^{-1/2} \tag{20}$$

Where $Pe_l = U_\infty l/\alpha$ is the number of Peclet. Comparing Eqs. (20) and (15), interesting results that relate δ_T and δ with the number of Prandtl $\Pr = \upsilon/\alpha$ are found,

$$\frac{\delta_T}{\delta} \rightarrow \Pr^{-1/2} >> 1 \tag{21}$$

The first consideration, $\delta << \delta_T$, therefore, is valid at the limit $\Pr^{1/2} << 1$, which is in the range of liquid metals. The heat transfer corresponding to low numbers of Prandtl is:

$$h \rightarrow \frac{k}{l} \Pr^{1/2} \operatorname{Re}_l^{1/2},\ \Pr << 1 \tag{22}$$

Or expressed with the Nusselt number $Nu = hl/k$:

$$Nu \rightarrow \Pr^{1/2} \operatorname{Re}_l^{1/2} \tag{23}$$

2. *The thickness of the thermal boundary layer* $\delta_T << \delta$. It is of interest the case of fluids with Prandtl numbers equal to 1 (the case of air), or greater than 1 (such as water or oils). As shown in Figure 16, the thickness of the thermal layer is assumed to be smaller than the thickness of the hydrodynamic boundary layer.

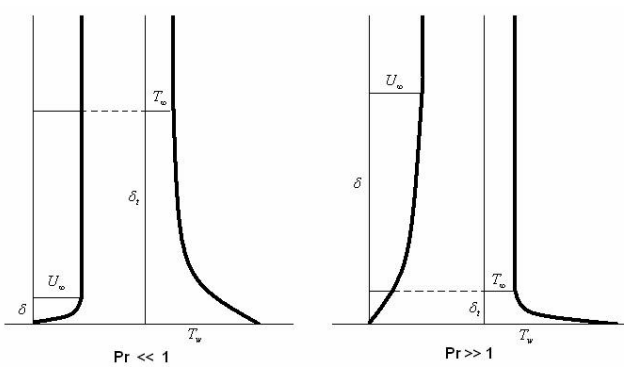

Figure 16. Effect of Pr in the thickness relative to the hydrodynamic and thermal boundary layers [6].

Geometrically, it is clear that the value of u in the layer δ_T is not U_∞, but

$$u \rightarrow U_\infty \frac{\delta_T}{\delta} \tag{24}$$

Substituting this value into the convection - conduction balance, we have:

$$\frac{\delta_T}{l} \rightarrow \Pr^{-1/3} \operatorname{Re}_l^{-1/2} \tag{25}$$

and therefore

$$\frac{\delta_T}{\delta} \rightarrow \Pr^{-1/3} << 1 \tag{26}$$

Thus, the condition $\delta_T << \delta$ is valid in the case of fluids with $\Pr^{1/3} >> 1$. The heat transfer coefficient and the Nusselt number vary as:

$$h \rightarrow \frac{k}{l} \Pr^{1/3} \operatorname{Re}_l^{1/2},\ \Pr >> 1 \tag{27}$$

$$Nu \rightarrow \Pr^{1/3} \operatorname{Re}_l^{1/2},\ \Pr >> 1 \tag{28}$$

where $Nu = hl/k$.

5. TEST CASE STUDY AND NUMERICAL SIMULATION

In the last decades, due to the increase in numerical techniques and the data processing capacity of computational resources, alternatives have emerged that cannot substitute experimentation, but allow results with very good approximation for the study of different phenomena. The technique that has emerged as a complement to the experimentation is called Computational fluid dynamics or CFD. This technique attempts to use computational resources to solve the mathematical equations of physical laws by numerical methods, which describe phenomena such as the movement of fluids and, and occasionally, other associated events such as heat transfer, chemical reactions, etc. Its benefits come mainly from the reduction of the number of experimental trials required and the time of development. In the results of these techniques, along with movement and pressure, variations in properties, forces exerted on adjacent solids, energy exchanges can be obtained. One of the important aspects, to support the results obtained through CFD, is the validation through experimental data. This

point is of vital importance, to give confidence to the results obtained. With the increase of commercial programs, a growing number of technicians have come into contact with these methods. However, the characteristics of the CFD are often not well known, and therefore the results may not be correct or useful. Therefore, it has become very important for the management of CFD, training in fluid dynamics and knowledge of the philosophy, capabilities and limitations of the system. FLUENT, is a commercial numerical simulation package which provides a wide range of numerical solutions to problems within the industry and research area, for this reason it will be used in this research.

5.1 Specifications of the simulated cases

In order to carry out the evaluation of the thermal influence in the development of the fluid, a series of cases to be solved numerically has been programmed, which are reflected in Table 1. In these cases, the nominal conditions of the fluid will be the same for all, varying only two parameters, the angle of incidence of the fluid on the airfoil and the surface temperature of the blade. The nominal conditions will be extracted from real operation data of a 12-stage axial compressor of a RUSTON model TB-5000 gas turbine [7].

Table 1. Test cases

Angle of attack	Surface temperature
0º	**510.90**
	410.90
	310.90
15º	**510.90**
	410.90
	310.90

For this particular case the scenario of the 12th stage will be analyzed as it presents the most critical pressure and temperature conditions of the fluid. In particular, the input data of the stator blading will be considered, because for this work the effects of rotation will not be evaluated. The operating conditions are shown in Table 2. Under these parameters, the Reynolds number can be calculated according to two characteristic lengths, the profile chord, and the distance perpendicular to the shortest flow direction of the passage. Table 3 shows the calculation of the Reynolds number as a function of the airfoil chord.

Table 2. Nominal parameters

Velocity	[m/s]	231.07
Pressure	[Pa]	579118.50
Temperature	[K]	510.90
Mach (Ma)		0.51

Table 3. Calculation of Reynolds number

	Characteristic length	Velocity (U)	PROPERTIES		Re
			Dynamic viscosity (μ)	**Density (ρ)**	
	[m]	[m/s]	[N s/m^2]	[Kg/m^3]	
Chord (c)	0.01984	231.07	2.7409E-05	3.9524	6.6108E+5

5.2 Airfoil in a two-dimensional cascade

In the 1930s, the NACA (National Advisory Committee for Aeronautics) designed a family of airfoils, which originated from the same equation:

$$\pm y = a_0 x^5 - a_1 x - a_2 x^2 + a_3 x^3 - a_4 x^4 \quad (29)$$

This equation is presented and discussed in the NACA Report No. 460 [8]. The chord c for the airfoils represented by this Equation (29) was 1 ft in length. The constants a_0, a_1, a_2, a_3, a_4 were evaluated by setting priorities. With these evaluations, Eq. (29) is transformed into the following expression:

$$\pm y = 0.2969x^5 - 0.12x - 0.3516x^2 + \ldots$$
$$\ldots + 0.2843x^3 - 0.1015x^4 \quad (30)$$

This equation defines only the basic sections. The work presented in [8], takes the basic section one step further, by introducing the maximum thickness t into Eq. (30), producing the following equation:

$$\pm y = 5t_{perfil}(0.2969x^5 - 0.12x - 0.3516x^2 + \ldots$$
$$\ldots + 0.2843x^3 - 0.1015x^4) \quad (31)$$

This equation sets the series of NACA 4-digit wing sections. Note that when the maximum thickness t

of the airfoil is 0.20 in Eq.(31), it returns to its previous expression (30). In general, these equations describe the airfoils in a basic form, being flexible to modifications according to the application. That is why some of the NACA airfoils are defined by a series of tabulated points due to these reforms. The airfoil to be used is the NACA 0012 (Figure 17). This profile has applications in areas of supersonic flow, considered a thin airfoil because the width-chord ratio is 12% ($t_{perfil}/c = 0.12$).

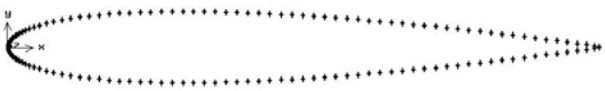

Figure 17. NACA 0012 airfoil.

The reason for using a symmetric profile such as the NACA 0012 is based on the fact of having experimental information in the literature, to carry out the validation of the numerical simulation, which will take place later. The NACA 0012 airfoil will be mounted in a two-dimensional cascade composed of three airfoils, in which the intermediate blade will be the object of study. The dimensional characteristics of this cascade are shown in Figure 18 and are based on the stator blading airfoil southern dimensions in the 12th stage of the axial compressor of the RUSTON model TB-5000 gas turbine.
The variations in the inflow direction according to the test cases will be done as indicated by the angle w shown in Figure 18.

5.3 Mesh generation

The mesh used in the solution of this case, is a structured mesh (Quad-Map), with elements basically quadrilateral, the same that was generated in GAMBIT®. The computational field of the mesh is shown in Figure 19, with the dimensions being plotted as a function of the airfoil chord. Also, the initially generated mesh contains 600 lines perpendicular to the airfoil surface (i) and 50 tangential lines (j), which generate the field nodes around the blade. Figures 20 and 21 show this configuration around the airfoil.

This structured mesh contains 4 types of boundaries, which are specified below and shown in Figure 22:
a) Input line
b) Periodicity lines
c) Airfoil limit wall lines
d) Output line

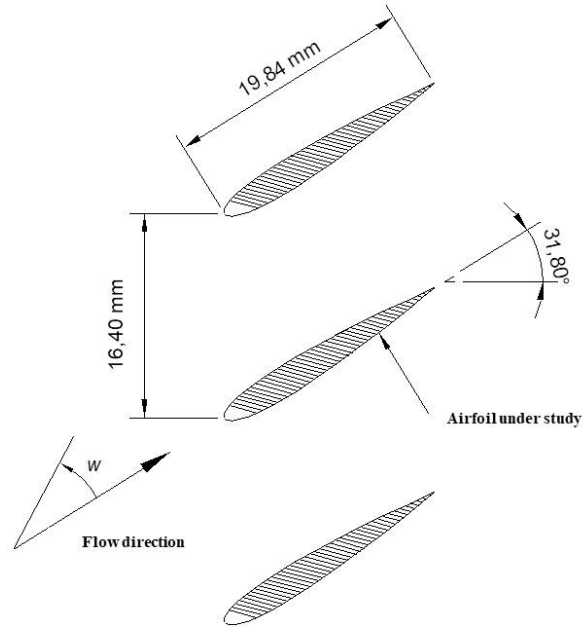

Figure 18. Configuration of the two-dimensional cascade

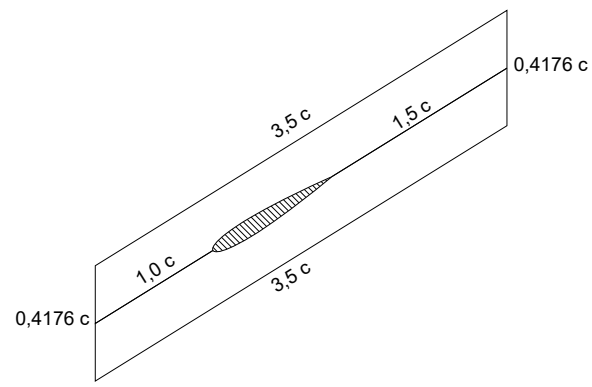

Figure 19. Computational field dimensions of the mesh.

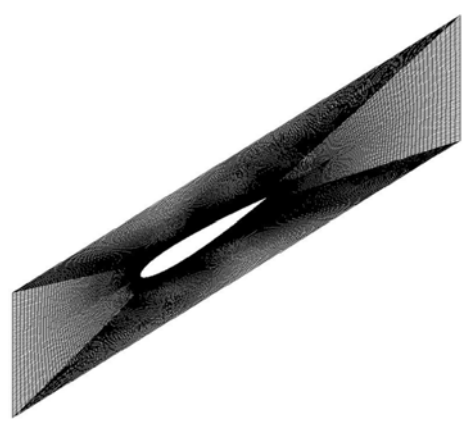

Figure 20. Structured mesh.

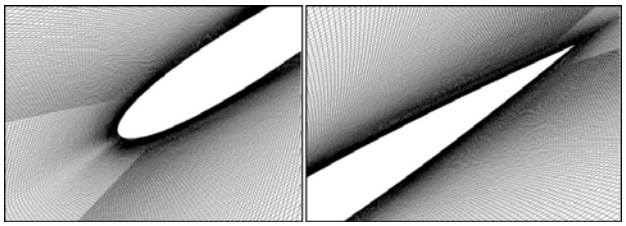

Figure 21 Structured mesh near the airfoil NACA 0012

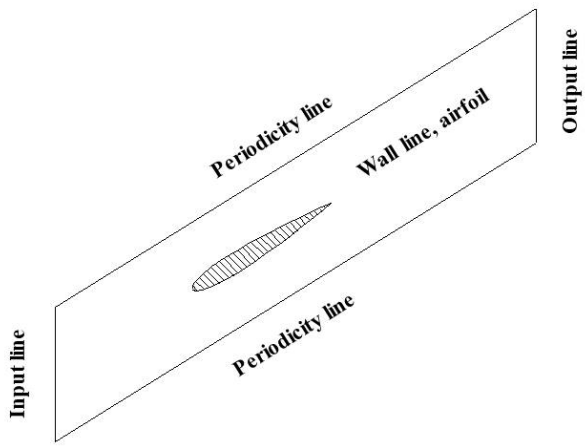

Figure 22. Structured mesh boundary around the NACA 0012 airfoil.

Mesh independence

The mesh independence process is performed in order to find an optimal number of nodes that ensures good results in a numerical simulation. The number of nodes used is proportional to the computational resources required, as well as to the execution time, so when optimizing the number of nodes, these parameters are improved. To carry out this process, it is necessary to compare the results obtained from the numerical simulation with different sizes of meshing. For this purpose, the numerical simulation of a specific case was carried out with 6 different mesh sizes, as specified in Table 4, varying j and maintaining constant i.

Table 4. Mesh sizes to evaluate

Mesh number	Dimensions (i, j)	Nodes
1	**600 x 50**	**30 000**
2	**600 x 100**	**60 000**
3	**600 x 150**	**90 000**
4	**600 x 200**	**120 000**
5	**600 x 250**	**150 000**
6	**600 x 300**	**180 000**

Two parameters have been taken into account in this process:

1. Velocity profile. The 10% of the blade chord will be considered on both the pressure side and suction side.
2. Mass flow. It will be determined along the fluid inlet and outlet line inside the mesh. This parameter is decisive, since it is governed by the law of conservation of mass.

The results obtained from the numerical simulations are compared in the graphs shown in Figures 23-26. As shown in Figures 23 and 24, the results obtained with the mesh of 600x50 nodes departs from the average of the rest, indicating that this number of nodes is not enough to yield good results. The use of a mesh of 600x100 nodes would give results with enough approximation to those of the 600x300 mesh nodes, the larger one, being feasible the use of this last mesh in the numerical solution of the case under study. However, when analyzing the graphs in Figures 25 and 26 in which the results of the inlet and outlet mass flow are presented, a separation of the mesh profiles of 600x50, 600x100 and 600x150 of the average of the last three meshes is shown. This indicates that it is not feasible to use the mesh of 600x100 nodes as previously considered. It is also possible to observe that the 600x200, 600x250 and 600x300 meshes are within a very approximate average range. Thus, the optimal mesh size is 600x200 for the solution of this case.

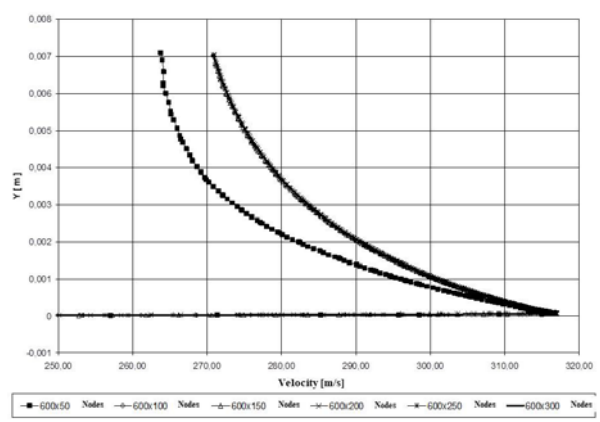

Figure 23. Velocity profile (10% of the blade chord on the airfoil pressure side)

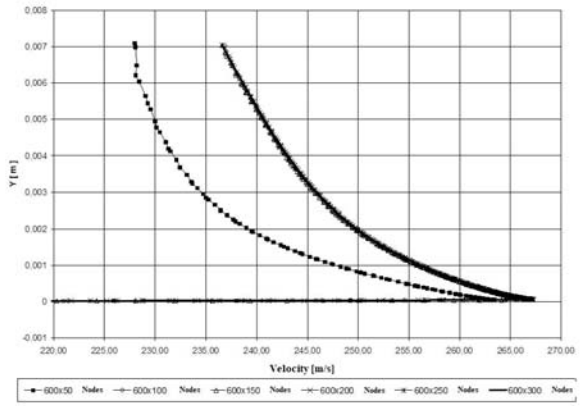

Figure 24. Velocity profile (10% of the blade chord on the airfoil suction side)

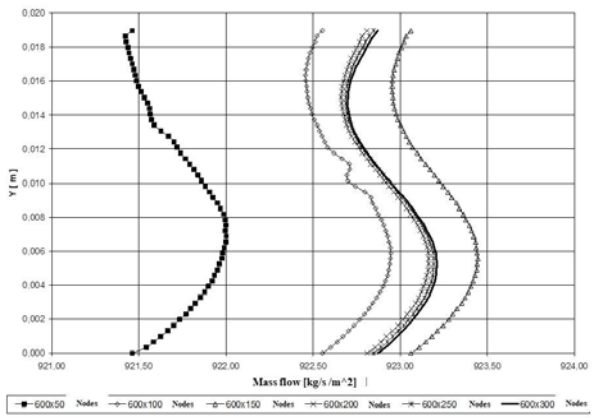

Figure 25. Mass flow profile (flow input line of the mesh)

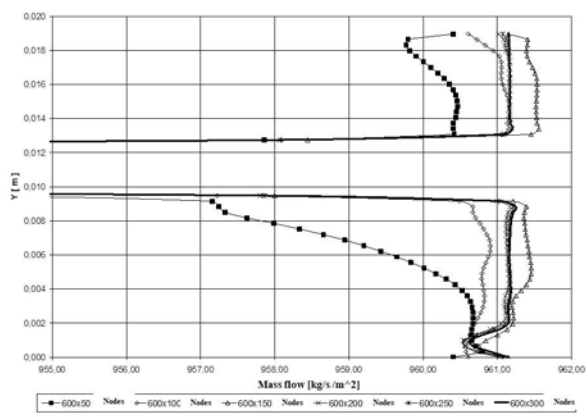

Figure 26. Mass flow profile (flow output line of the mesh)

5.4 Numeric solution method

FLUENT allows selecting a method of solution, segregated or coupled, which solve the integral equations for the conservation of mass and momentum, energy, turbulence and chemical species. In both cases, the technique is based on control volume, consisting of:

• Division of the domain into discrete control volumes using a computational mesh.
• Integration of equations into individual control volumes to construct algebraic equations for the discretization of (unknown) dependent variables such as velocity, pressure, temperature, and conserved values.
• Linearization of the discretized equations and solution of the linear system of linear equations to produce updated values of the dependent variables.

Both numerical methods employ a similar discretization process, but the approximation used to linearize and solve the discretized equations is different. In our case the segregated solution method will be used, since it is more convenient to the purpose and offers a lesser convergence time to the coupled one. Within the numerical solution methods, there are also two ways of linearizing the equations:

Implicit: For a given variable, the unknown variable in each cell is calculated using a relation that includes both known and unknown variables of neighboring cells. Therefore, each unknown variable will appear in more than one equation in the system, and these equations must be solved simultaneously to give the unknown quantities.

Explicit: For a given variable, the unknown variable in each cell is calculated using a relation that includes only existing values. Therefore each unknown variable will only appear in an equation in the system and the equations for the unknown variable in each cell can be solved one at a time to give the unknown quantities.

In the segregated solution method, each discrete equation is implicitly linearized with respect to which dependent variable has the equation. This will result in a system of linear equations with an equation for each cell in the domain. Because there is only one equation per cell, this is sometimes called a "scalar" system of equations. It is used in conjunction with a multi-mesh algebraic method (AMG) to solve the resulting system of equations for the dependent variable in each cell. For example, the momentum equation in x is linearized to produce a

system of equations in which the velocity u is unknown. The simultaneous solution of the equation system (using the AMG solution) produces an updated velocity field. In summary, the approximate segregated solution for a single variable field is considered for all cells at the same time. This then resolves the next variable field to again consider all the cells at the same time. And so on. In the case of the segregated solution method, there is no explicit option.

Segregated solution method
Using this approximation method, the equations are solved sequentially (segregated from each other), because the equations are nonlinear (and coupled), several iterations of the solution must be developed before obtaining solution convergence. Each iteration consists of the steps explained below.

1. The properties of the fluid are updated based on the current solution. (At the beginning of the iterations, the properties are updated according to the initial values).

2. The moment equations for u, v, and w are solved each in turn using current values for pressure and mass flow, to update the velocity fields.

3. From the velocities obtained in step 2, it may be that the continuity equation is not satisfied locally, a "Poisson-type" equation for the pressure correction is derived from the continuity equation and the linearized momentum equation. This pressure correction equation is subsequently solved to obtain the necessary corrections for the pressure and velocity fields and the mass flow until the continuity is satisfied.

4. If necessary, the equations of turbulence, energy, species and radiation are solved using the previously updated values of the other variables.

5. When the interface coupling is included, the source terms in the appropriate continuous phase equations can be updated with the discrete phase path calculation.

6. A review of the convergence criterion of the equation is performed.

These steps are wrapped in a cycle, until the convergence criterion is met.

5.5 Turbulence model
FLUENT provides the following turbulence models:
• Spalart-Allmaras model
• k-ϵ models
  -Standard k-ϵ model
  -Renormalization-group (RNG) k-ϵ model
  -Realizable k-ϵ model
• k-ω models
  -Standard k-ω model
  -Shear-stress transport (SST) k-ω model
• v^2-f model
• Reynolds stress model (RSM)
• Large eddy simulation (LES) model

Unfortunately there is no universally accepted model of turbulence for the solution of all kinds of problems, this is why the selection of the turbulence model depends on the considerations and the physical properties of the fluid, the practice that is acquired for the resolution of a particular type of problem, the level of accuracy required, available computational resources, and the amount of time allotted for the simulation. To make the most appropriate selection for an application, we need to understand the capabilities and limitations of all the options.

FLUENT groups the models into: zero-equation, one-equation and two-equation models. To understand the difference between them, it is important to know that it is assumed from the hypothesis that if a fluid can have laminar viscosity μ, then a turbulent flow must have turbulent viscosity μ_t. A zero-equation model establishes a constant value for the turbulent viscosity (or deduces it as an algebraic function of the flow parameters). A one-equation model uses a differential equation to predict a part of the turbulent viscosity, whereas a two-equation model employs two differential equations.

One-equation model
The Spalart-Allmaras model is relatively simple, with an equation that solves the modeled transport equation for turbulent viscosity. This model was

especially designed for aerospace applications related to limited wall flow and has given good results for boundary layers subjected to adverse pressure gradients. It also has popularity of turbomachinery flow applications. It is a more effective model for cases with low Reynolds numbers, although it has been evaluated in ranges of hypersonic flow by Paciorri [9] giving excellent results. In FLUENT the Spalart-Allmaras model has been employed with contour functions where the resolution of the mesh is not good enough. This allows us to consider it a good option to obtain relatively large simulations with not very fine meshes in which the calculation with turbulent flow is not expected to be very critical. In addition, the gradients near the walls of the transported variable in the model are smaller than the gradients of the variables in the models $k-\varepsilon$, which makes the model less sensitive to numerical errors when the structured meshes are used near the walls. The Spalart-Allmaras model does not predict certain behavior of turbulent, isotropic and homogeneous flows, so it is not known to what extent it is required in complex fluids. In addition, single-equation models are criticized for their inability to accommodate rapidly to changes in scale lengths, for example when the flow passes from a zone bounded by walls to a free zone flow. This model has a good prediction of the coefficient of friction and the flow velocity profiles on surfaces under compressible flow conditions [10].

Two-equation model

Standard k-epsilon model: It is a simple model of two equations, where the solution of two separate transport equations leads to independent determination of turbulent velocity and scale lengths. The Standard k-epsilon model is robust, economical and of reasonable approximation for a very wide range of turbulent flows; for that reason has great popularity in industrial flows and heat transfer simulations. It is a semi-empirical model; the equations of the model are derived from phenomenological and empirical considerations and, since this model was known, improvements have been introduced. In FLUENT you can choose two variants of this model:

Realizable k-epsilon: This model is of relatively recent development and, compared to the Standard k-epsilon model, is an alternative formulation for turbulent viscosity and there is a new transport equation for the dissipation ratio. The term "realizable" means that the model satisfies certain mathematical constraints for Reynolds stress, according to the physics of turbulent flow. Neither the Standard $k-\varepsilon$ model nor the RNG $k-\varepsilon$ model are realizable. The immediate benefit of the realizable model is that it has a higher resolution for flows including rotation, boundary layers under strong and adverse pressure gradients, separation and recirculation. Both the RNG k-epsilon model and the realizable model present remarkable advances on the Standard model where the flow characteristics include strong curvatures, vortices and rotations. As the model is relatively new, it is not clear when the realizable k-epsilon model surpasses the RNG model, although in initial studies it has been shown to give better results and behavior compared to other versions of k-epsilon models in the case of separate flows and complex secondary flows.

RNG k-epsilon: The k-epsilon equations are derived from the application of a very rigorous statistical technique (renormalization group method) to the Navier-Stokes instantaneous equations. It is very similar in form to the standard k-epsilon equations but includes: an additional term that improves the analysis of rapidly forced flows, the effect of eddies on turbulence (thereby increasing accuracy for heavily removed flows) and an analytical formula for turbulent numbers of Prandtl. In addition, the k-epsilon model works with high Reynolds numbers, whereas the RNG theory gives a differential formula derived analytically by the effective viscosity also valid for low Reynolds numbers. It should also be said that the effectiveness of this feature depends on an adequate treatment in the areas close to the walls. These characteristics make the RNG model usable for a wide range of flows, higher than the standard k-epsilon model.

Reynolds Stress Model (RMS): This model is the most elaborate model provided by FLUENT and has a high potential to predict complex flows in detail, since it takes into account the effects of curvature, eddies, rotation and rapid changes of forced flows in a more rigorous way than the models of one or two equations. That is, instead of assuming an equal

turbulent viscosity in the three spatial directions, consider a Reynolds voltage model for each of the six Reynolds stress terms. The stability of the convergence is a serious problem and the computation time is much higher than in the two-equation models. In addition, RMS does not always produce superior results over simpler models. However, using RMS is imperative when the characteristics of the flow of interest are the result of anisotropy. Examples may include cyclic flows, many vortex flows in combustion chambers, rotary flow transit and secondary flow in conduits.

Large Eddy Simulation (LES): A very good solution for turbulent flows in time-dependent Navier-Stokes equations for turbulent flows with high Reynolds numbers and complex geometries has not yet been found. There are two alternative methods for transforming the Navier-Stokes equation so that small-scale turbulence fluctuations do not take into account: "Reynold averaging" and "Filtering". Both methods introduce two additional methods into the calculation equations to be obtained to arrive at the solution. The Reynold-Averaged Navier-Stokes (RANS) equations represent transport equations only for mean flow quantities. The approximation made in considering only these average flow variables considerably reduces the computational effort. If the mean flow is steady the steady state solution will be obtained economically. The Reynold-average approximation is generally adopted for practical engineering calculations and uses models such as Spalart-Allmaras, k-epsilon and RMS (Reynold Stress Model). LES is the other alternative; the swirls are calculated with simulations depending on the time from equations that filter those swirls smaller than the measurement of the filter. The filtration is mainly based on manipulating the exact Navier-Stokes equation and deleting only the smallest eddies of a measurement (the mesh measurement). This process also generates, as the Reynolds averaging, additional terms. The attraction of LES is that it allows reducing the error induced by the turbulence model. The applications of the LES model in industrial fluid simulations are still very early, whose typical applications are reduced to simple geometries due to their high computational cost to solve the equations. Discretization must be taken into account, since the loss of accuracy is rapid if it is not performed correctly. In addition, the contour functions with LES still need to be validated.

LES approaches are currently under investigation and are only available for testing if computer tools are available to perform the appropriate calculations. Therefore as a general rule it is recommended that conventional turbulence models use the Reynolds-average approximation in the practical calculations.
Due to the characteristics of the models discussed above, the one-equation Spalart-Allmaras turbulence model is selected for the solution of this case. The mathematical model, with its respective variables, is presented below.

Spalart-Allmaras turbulence model
The model proposed by Spalart and Allmaras [11] solves a transport equation for an amount that is a modified form of turbulent kinematic viscosity. The variable to be carried in the model Spalart-Allmaras, $\tilde{\nu}$, is identical to the turbulent kinematic viscosity, except in the region near the wall (affected by viscous effects). The transport equation for $\tilde{\nu}$ is:

$$\frac{\partial}{\partial t}(\rho\tilde{\nu})+\frac{\partial}{\partial x_i}(\rho\tilde{\nu}u_i)=G_\nu+\frac{1}{\sigma_{\tilde{\nu}}}\left[\frac{\partial}{\partial x_j}\left\{(\mu+\rho\tilde{\nu})\frac{\partial\tilde{\nu}}{\partial x_j}\right\}+C_{b2}\rho\left(\frac{\partial\tilde{\nu}}{\partial x_j}\right)^2\right]-\ldots$$
$$\ldots-Y_\nu+S_{\tilde{\nu}} \qquad (32)$$

where G_ν is the production of turbulent viscosity, Y_ν is the destruction of the turbulent viscosity occurring in the region near the wall due to wall locking and viscous damping. $\sigma_{\tilde{\nu}}$ and C_{b2} are constant and ν is the molecular kinematic viscosity. $S_{\tilde{\nu}}$ is a term defined by the user. Note that since turbulent kinetic energy K is not calculated in the Spalart - Allmaras model, the last term in Eq. (32) is ignored when Reynolds stresses are estimated.

CONCLUSIONS

It is important to know the properties of the working fluid within any engineering process, as well as the variation they present with respect to the conditions of operation, in order to predict their behavior and the process of energy change that suffers the working fluid. Based on this idea, the intention of the paper was to present a theoretical analysis, as a

first part of a complete study on thermal influence on airfoil hydrodynamic boundary layer. The principles analyzed deal with rotating compressor stall, and hydrodynamic and thermal boundary layer foundations. In a second part, we specified the dimensional characteristics of the linear blade cascade and its operating conditions, the mesh generation and the analysis performed to determine the optimum size employed, as well as the selection of the turbulence model and the start parameters of the simulation. An analysis of the results will be presented, showing the fields generated around the waterfall of velocity, pressure and temperature, as well as velocity profiles in different points of the profile surface showing the thermal influence on the development of the hydrodynamic boundary layer.

REFERENCES

[1] P. Boyce, Meherwan "Gas turbine engineering handbook", Gulf Publishing Company, first edition, 1982, p 603

[2] W. R. Hawthorne "Aerodynamics of turbines and compressors" Board, first, 1964, p 616

[3] Greitzer, E. M., "The Stability of Pumping Systems," J. Fluids Engineering, Vol.103, pp. 193-242, June 1981

[4] Emmons, H. W., Pearson, C. E., andGrant, H. P.,Compressor Surge and Stall Propagation, Trans. A. S. M. E.,77, 455–467 (1955).

[5] P. Incropera, Frank / P. De UIT, David "Introduction to Heat Transfer " John Wiley &Sons, third edition, 1996, p 795

[6] Bejan, Adrian " Convection heat transfer ", John Wiley & Sons, Inc., second edition, 1995, p 623

[7] Rodríguez Dávalos, Jesús "Recuperación de álabes del compresor de turbina de gas marca RUSTON modelo TB-5000" Report, PEMEX, 1999

[8]Jacobs, Eastman N., Ward, Kenneth E., and Pinkerton, Robert M.:"The Characteristics of 78 Related Airfoil Sections from Tests in the Variable density Wind Tunnel" NACA Rept. No. 460, 1932.

[9] Paciorri R., Dieudonné W., "Validation of the Spalart-Allmaras turbulence model for application in hypersonic flows", Von Karman Institute for fluid Dynamics, Sint-Genesius-Rode, Belgium, 1997

[10] Bardina J.E., Huang P.G., Coakley T.J., "Turbulence modeling validation, testing, y development" NASA Technical Memorandum 110446, National Aeronautics and Space Administration, 1997

[11] P. Spalart and S. Allmaras, "A one-equation turbulence model for aerodynamic flows" Technical Report AIAA-92-0439, American Institute of Aeronautics and Astronautics, 1992.